Paper 181

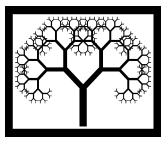

Proceedings of the Eleventh International Conference
on Computational Structures Technology,
B.H.V. Topping, (Editor),
Civil-Comp Press, Stirlingshire, Scotland

A Quadratic Ten Node Tetrahedral Cosserat Point Element for Nonlinear Elasticity

M. Jabareen[1], E. Hanukah[2] and M.B. Rubin[2]
[1]Faculty of Civil and Environmental Engineering
[2]Faculty of Mechanical Engineering
Technion-Israel Institute of Technology, Haifa, Israel

Abstract

It is known that the standard full integration ten node tetrahedral element is inaccurate for thin nearly incompressible structures. The objective of this work is to develop a ten node tetrahedral Cosserat Point Element (CPE) for nonlinear isotropic hyperelastic materials. Hyperelastic constitutive equations for the CPE are developed by treating the element as a structure with a strain energy function that is restricted to satisfy a nonlinear form of the patch test. A number of examples are considered which demonstrate that the resulting CPE is accurate and robust.

Keywords: Cosserat point element, hyperelasicity, quadratic, tetrahedral element.

1 Introduction

It is well known that generating a mesh for a general three-dimensional region is easier using tetrahedral elements than using brick elements. However, homogeneously deformable four node tetrahedral elements exhibit stiff response to bending and severe volumetric locking for nearly incompressible materials. Therefore, a number of element technologies have been proposed to improve the performance of the four node tetrahedral element for nearly incompressible materials ([1], [2], [3], [4], [5], [6]). Although the aforementioned technologies have improved the performance of the low order tetrahedral element for nearly incompressible materials, the performance for bending dominated deformations is still very poor.

Quadratic tetrahedral elements based on quadratic shape functions with full integration eliminate stiffness to bending modes but are known to exhibit inaccurate response for nearly incompressible materials. Mixed methods can be used for nearly incompressible materials, but they exhibit soft response to bending. Moreover, ABAQUS [7] has developed an undocumented patented element (C3D10M) called a modified

ten node tetrahedral element which is used to replace the full integration element for contact problems. However, that modified element exhibits unphysical instabilities in some problems. To the best of our knowledge, there are only a few technologies that have been proposed in the literature for improving the performance of the quadratic tetrahedral element for nearly incompressible materials which retain accuracy for bending deformations and are applicable to large deformations. Specifically, Lo and Ling [8] developed an improved 10-node tetrahedral element based on relaxing the compatibility condition for the constant strain term. The element stiffness matrix was separated into two parts, namely the constant strain term and the higher-order strain term. The incompressibility condition was imposed on the higher-order strain term in order to enhance the accuracy of 10-node tetrahedral element for nearly incompressible materials. However, their formulation is valid only for linear elasticity.

Another element technology produces a class of Cosserat Point Elements (CPEs) which are based on the theory of a Cosserat Point ([9], [10], [11], [12] [13], [14], [15], [16], [17]). In standard Bubnov-Galerkin methods a kinematic approximation is assumed to be valid pointwise in the element and it is used at the Gauss points of integration to the determine element stiffnesses. In contrast, in the CPE approach the kinematic approximation is only used to connect nodal director vectors (i.e. nodal positions) to element director vectors. Specifically, the hyperelastic constitutive equations of the CPE are developed by treating the element as a structure with a strain energy function that models the response of the structure to all modes of deformation. In particular, the nodal forces are related to derivatives of the strain energy function through algebraic relations in a similar manner to the relationship of the stress to derivatives of the strain energy function in the full three-dimensional theory of hyperelastic materials.

The objective of this paper is to discuss a ten node tetrahedral Cosserat Point Element (CPE) for three-dimensional deformations of nonlinear isotropic hyperelastic materials. The strain energy of the resulting CPE is restricted to satisfy a nonlinear form of the patch test and analytical expressions for the coefficients of the inhomogeneous strain energy have been determined to produce accurate results which are nearly insensitive to irregularity of the reference geometry of the CPE. Examples show that this CPE is both accurate and robust and that it an be used for thin structures and for nearly incompressible materials.

2 Basic equations of the CPE using the Bubnov-Galerkin approach

Figure 1 shows a sketch of a ten node 3-D tetrahedral CPE. Here, and throughout the text a superposed $(^*)$ is used to denote some quantities related to the three-dimensional which have counterparts in the CPE. A material point in the reference and deformed configurations is characterized by the convected coordinates $\theta^i \quad (i = 1, 2, 3)$

and is located by the position vector $\mathbf{X}^*$ and $\mathbf{x}^*$, respectively, defined by

$$\mathbf{X}^* = \sum_{j=0}^{9} N^j(\theta^i)\mathbf{D}_j, \quad \mathbf{x}^* = \sum_{j=0}^{9} N^j(\theta^i)\mathbf{d}_j(t) \tag{1}$$

where $\mathbf{D}_j$ are constant element director vectors, $\mathbf{d}_j(t)$ are the present values of the element directors, t is time, and N^j are tri-linear shape functions

$$\begin{aligned} &N^0 = 1, \quad N^1 = \theta^1, \quad N^2 = \theta^2, \quad N^3 = \theta^3, \\ &N^4 = \theta^1\theta^2, \quad N^5 = \theta^1\theta^3, \quad N^6 = \theta^2\theta^3, \\ &N^7 = \theta^1\theta^1, \quad N^8 = \theta^2\theta^2, \quad N^9 = \theta^3\theta^3, \end{aligned} \tag{2}$$

The tetrahedral region P is bounded by the four surfaces ∂P_J $(J = 1, 2, 3, 4)$ defined by (Fig. 1)

$$\begin{aligned} &-\frac{1}{4} \le \theta^1 \le \frac{1}{4} - \theta^2 - \theta^3, \quad -\frac{1}{4} \le \theta^2 \le \frac{1}{2} - \theta^3, \quad -\frac{1}{4} \le \theta^3 \le \frac{3}{4}, \\ &\theta^1 = -\frac{1}{4} \ \text{ on } \ \partial P_1, \quad \theta^2 = -\frac{1}{4} \ \text{ on } \ \partial P_2, \quad \theta^3 = -\frac{1}{4} \ \text{ on } \ \partial P_3, \quad , \\ &-\frac{1}{4} + \theta^1 + \theta^2 + \theta^3 = 0 \ \text{ on } \ \partial P_4, \end{aligned} \tag{3}$$

Also, the triads $\mathbf{D}_i$ and $\mathbf{d}_i$ $(i = 1, 2, 3)$ are restricted to be linearly independent with

$$D^{1/2} = \mathbf{D}_1 \times \mathbf{D}_2 \cdot \mathbf{D}_3 > 0, \quad d^{1/2} = \mathbf{d}_1 \times \mathbf{d}_2 \cdot \mathbf{d}_3 > 0 \tag{4}$$

The reciprocal vectors $\mathbf{D}^i$ and $\mathbf{d}^i$ are defined by

$$\mathbf{D}^i \cdot \mathbf{D}_j = \delta^i_j, \quad \mathbf{d}^i \cdot \mathbf{d}_j = \delta^i_j \quad \text{for} \quad (i, j = 1, 2, 3) \tag{5}$$

where δ^i_j is the Kronecker delta symbol.

Using these representations it is possible to determine the reference base vectors $\mathbf{G}_i$, their reciprocal vectors $\mathbf{G}^i$, the present base vectors $\mathbf{g}_i$, their reciprocal vectors $\mathbf{g}^i$ and the velocity field $\mathbf{v}^*$, such that

$$\begin{aligned} &\mathbf{G}_i = \mathbf{X}^*_{,i}, \quad \mathbf{G}^i \cdot \mathbf{G}_j = \delta^i_j, \quad (i, j = 1, 2, 3), \quad G^{1/2} = \mathbf{G}_1 \times \mathbf{G}_2 \cdot \mathbf{G}_3, \\ &\mathbf{g}_i = \mathbf{x}^*_{,i}, \quad \mathbf{g}^i \cdot \mathbf{g}_j = \delta^i_j, \quad (i, j = 1, 2, 3), \quad g^{1/2} = \mathbf{g}_1 \times \mathbf{g}_2 \cdot \mathbf{g}_3, \\ &\mathbf{v}^* = \dot{\mathbf{x}}^* = \sum_{j=0}^{9} N^j \mathbf{w}_j, \quad \mathbf{w}_j = \dot{\mathbf{d}}_j \end{aligned} \tag{6}$$

where a comma denotes partial differentiation with respect to θ^i, a superposed $(\dot{})$ denotes material time differentiation holding θ^i fixed and $\mathbf{w}_j$ are the director velocities.

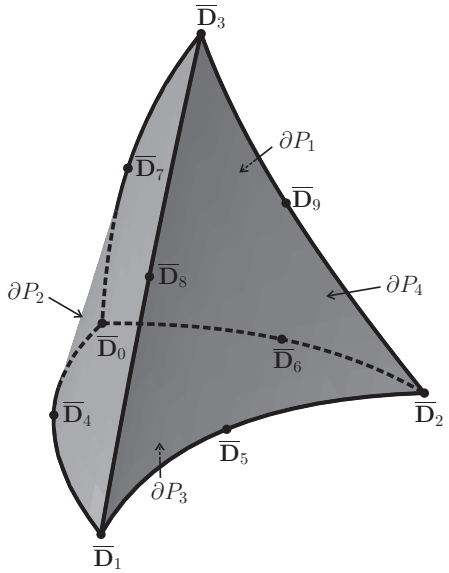

Figure 1: Sketch of a quadratic tetrahedral element showing the 10 nodal directors $\overline{\mathbf{D}}_i$ $(i = 0, 1, ..., 9)$ and the surface ∂P_J.

For the CPE it is convenient to define a deformation tensor $\mathbf{F}$ associated with homogeneous deformations and deformation vectors $\boldsymbol{\beta}_i$ associated with inhomogeneous deformations by

$$\mathbf{F} = \sum_{i=1}^{3} \mathbf{d}_i \otimes \mathbf{D}^i, \quad \boldsymbol{\beta}_i = \mathbf{F}^{-1}\mathbf{d}_{i+3} - \mathbf{D}_{i+3}, \quad (i = 1, ..., 6) \tag{7}$$

It then can be shown that the three-dimensional deformation gradient $\mathbf{F}^*$ associated with the kinematic assumption (6) is given by

$$\mathbf{F}^* = \mathbf{F}\left(\mathbf{I} + \sum_{i=1}^{3}\sum_{j=1}^{6} N_{,i}^{j+3}\boldsymbol{\beta}_j \otimes \mathbf{G}^i\right) \tag{8}$$

¿From this expression it can be deduced that $\boldsymbol{\beta}_i$ are pure measures of inhomogeneous deformations since when they vanish $\mathbf{F}^* = \mathbf{F}$ is independent of the coordinates θ^i.

It is well known (e.g. [18]) that the conservation of mass and the balance of linear momentum can be expressed in the forms

$$\rho^* g^{1/2} = \rho_0^* G^{1/2}, \quad \rho^* \dot{\mathbf{v}}^* = \rho^* \mathbf{b}^* + div^* \mathbf{T}^* \tag{9}$$

where ρ_0^* and ρ^* are the reference and current values of the mass density, respectively, $\mathbf{b}^*$ is the body force per unit mass, $\mathbf{T}^*$ is the Cauchy stress tensor. Multiplying $(9b)$ by $g^{1/2}$ and using the identity $\left(g^{1/2}\mathbf{g}^j\right)_{,j} = \mathbf{0}$, the conservation of mass and the balance

of linear momentum can be written in the alternative forms

$$
\begin{aligned}
&m^* = \rho^* g^{1/2} = m^*(\theta^i),\\
&m^*\dot{\mathbf{v}}^* = m^*\mathbf{b}^* + \sum_{j=1}^{3} \mathbf{t}^{*j}_{,j}, \quad \text{with} \quad \mathbf{t}^{*j} = g^{1/2}\mathbf{T}^*\mathbf{g}^j, \quad (j = 1,2,3)
\end{aligned}
\tag{10}
$$

Next, the Bubnov-Galerkin weak form of the balance of linear momentum can be obtained by multiplying (10b) by the shape functions N^i and integrating over the material region P^* with closed smooth boundary ∂P^* such that

$$
\sum_{j=0}^{9} m y^{ij}\dot{\mathbf{w}}_j = m\mathbf{b}^i + \mathbf{m}^i - \mathbf{t}^i, \quad (i = 0,1,...,9) \quad \text{with} \quad \mathbf{t}^0 = \mathbf{0} \tag{11}
$$

These equations are the same as the director momentum equations of the CPE where the mass m, director inertia quantities y^{ij}, external director couples $\mathbf{b}^i$ due to body forces and external director couples $\mathbf{m}^i$ due to surface tractions are defined by

$$
\begin{aligned}
&m = \int_{P^*} \rho^* dv^*, \quad m y^{ij} = \int_{P^*} N^i N^j \rho^* dv^* = m y^{ji},\\
&m\mathbf{b}^i = \int_{P^*} N^i \rho^* \mathbf{b}^* dv^*, \quad \mathbf{m}^i = \int_{\partial P^*} N^i \mathbf{t}^* dv^*
\end{aligned}
\tag{12}
$$

In these expressions dv^* is the current element of volume, da^* is the current element of area, $\mathbf{t}^*$ is the traction vector applied to the surface ∂P^* and use has been made of conservation of mass which yields

$$
\dot{m} = 0, \quad \dot{y}^{ij} = 0 \tag{13}
$$

The intrinsic director couples $\mathbf{t}^i$, which require constitutive equations, will be defined later. The balance of angular momentum is satisfied provided that the tensor $\mathbf{T}$ is symmetric

$$
\mathbf{T} = d^{-1/2} \sum_{i=1}^{9} \mathbf{t}^i \otimes \mathbf{d}_i = \mathbf{T}^T \tag{14}
$$

Moreover, it can be shown the $\mathbf{T}$ is related to the volume averaged Cauchy stress [16]

$$
d^{1/2}\mathbf{T} = \int_{P^*} \mathbf{T}^* dv^* \tag{15}
$$

For a three-dimensional hyperelastic solid a strain energy function Σ^* and the Cauchy stress tensor $\mathbf{T}^*$ are proposed of the form

$$
\Sigma^* = \widehat{\Sigma}(\mathbf{C}^*), \quad \mathbf{C}^* = \mathbf{F}^{*T}\mathbf{F}^*, \quad \mathbf{T}^* = 2\rho^*\mathbf{F}^* \frac{\partial \widehat{\Sigma}(\mathbf{C}^*)}{\partial \mathbf{C}^*} \mathbf{F}^{*T} \tag{16}
$$

Thus, within the context of the Bubnov-Galerkin approach with full integration the constitutive equations for the intrinsic director couples $\mathbf{t}^i$ can be determined by numerically evaluating an integral which weights the Cauchy stress $\mathbf{T}^*$ by gradients of the shape functions N^i. Specifically, for a given strain energy function Σ^*, it is assumed that the kinematic approximation (1) for $\mathbf{F}^*$ is valid pointwise and that $\mathbf{T}^*$ is determined by the expressions (16) at each Gauss point in the element.

3 Constitutive equations of the CPE using the direct approach

Within the context of the direct approach, the kinematics of the CPE are characterized by introducing reference element director vectors $\mathbf{D}_i$ and their present values $\mathbf{d}_i$

$$\{\mathbf{D}_i,\, \mathbf{d}_i(t)\}, \quad (i = 0, 1, ..., 9) \tag{17}$$

which satisfy the restrictions (4). Then, the conservation of mass and the balances of director momentum are proposed in the forms (13) and (11), respectively.

Constitutive equations for the intrinsic director couples $\mathbf{t}^i$ of a hyperelastic CPE are determined by procedures similar to those in the three-dimensional theory. Specifically, the CPE is considered to be a structure and the resistance to all deformational modes of the structure is characterized by a strain energy Σ (per unit mass) of the structure of the form

$$\Sigma = \Sigma(\mathbf{C},\, \boldsymbol{\beta}_i), \quad \mathbf{C} = \mathbf{F}^T\mathbf{F} \tag{18}$$

Moreover, it is convenient to introduce the rate of dissipation D by the form

$$\mathsf{D} = \mathsf{W} - \dot{\mathsf{K}} - m\dot{\Sigma} \geq 0 \tag{19}$$

where the rate of external work W done on the CPE and its kinetic energy K are defined by

$$\mathsf{W} = \sum_{i=0}^{9}(m\mathbf{b}^i + \mathbf{m}^i)\cdot\mathbf{w}_i, \quad \mathsf{K} = \frac{1}{2}\sum_{i=0}^{9}\sum_{j=0}^{9} m y^{ij}\mathbf{w}_i\cdot\mathbf{w}_j \tag{20}$$

Then, with the help of (11), (13), and (15) the rate of dissipation (19) can be rewritten in the form

$$\mathsf{D} = d^{1/2}\mathbf{T}\cdot\mathbf{D} + \sum_{i=1}^{6}\mathbf{F}^T\mathbf{t}^{i+3}\cdot\dot{\boldsymbol{\beta}}_i - m\dot{\Sigma} \geq 0 \tag{21}$$

where $\mathbf{D}$ is the symmetric part of the rate tensor $\mathbf{L}$ defined by

$$\mathbf{L} = \dot{\mathbf{F}}\mathbf{F}^{-1} = \sum_{i=1}^{3}\mathbf{w}_i\otimes\mathbf{d}^i, \quad \mathbf{D} = \frac{1}{2}\Big(\mathbf{L} + \mathbf{L}^T\Big) \tag{22}$$

For an elastic CPE the rate of dissipation vanishes for all processes so that standard methods can be used to deduce that the kinetic quantities are related to derivatives of Σ, such that

$$
\begin{aligned}
&d^{1/2}\mathbf{T} = 2m\mathbf{F}\frac{\partial \Sigma}{\partial \mathbf{C}}\mathbf{F}^T, \quad \mathbf{t}^{i+3} = \mathbf{F}^{-T}\frac{\partial \Sigma}{\partial \boldsymbol{\beta}_i}, \quad (i = 1, 2, ..., 6), \\
&\mathbf{t}^0 = \mathbf{0}, \quad \mathbf{t}^i = \left(d^{1/2}\mathbf{T} - \sum_{j=4}^{9} \mathbf{t}^j \otimes \mathbf{d}_j \right) \cdot \mathbf{d}^i, \quad (i = 1, 2, 3)
\end{aligned}
\tag{23}
$$

3.1 Restrictions associated with a nonlinear form of the patch test

In [13] restrictions on the strain energy Σ of the CPE were developed which ensure that the CPE will reproduce exact solutions for all homogeneous deformations of a uniform homogeneous anisotropic elastic material for all reference element shapes. Specifically, it was shown there that these restrictions will be satisfied if Σ is related to the strain energy function Σ^* of the three-dimensional material such that

$$
m\Sigma(\mathbf{C}, \boldsymbol{\beta}_i) = \Sigma^*(\overline{\mathbf{C}}) + \Psi(\boldsymbol{\beta}_i, \mathbf{D}_i), \quad \overline{\mathbf{C}} = \overline{\mathbf{F}}^T\overline{\mathbf{F}} \tag{24}
$$

where $\overline{\mathbf{F}}$ is the average deformation gradient (see [14]) defined by

$$
\overline{\mathbf{F}} = \frac{1}{V}\int_{P_0^*} \mathbf{F}^* \, dV^* = \mathbf{F}\left(\mathbf{I} + \sum_{j=1}^{6} \boldsymbol{\beta}_j \otimes \mathbf{V}^j \right) \tag{25}
$$

and the vectors $\mathbf{V}^i$ are determined by the reference geometry of the CPE

$$
V^*\mathbf{V}^j = \sum_{i=1}^{3} \int_{P_0^*} N_{,i}^{j+3}\mathbf{G}^i dV^*, \quad (j = 1, 2, ..., 6), \quad V^* = \int_{P_0^*} dV^* \tag{26}
$$

Here, Ψ represents the strain energy per unit mass of inhomogeneous deformations which for the CPE includes bending, torsional and higher-order hourglass modes of deformation. Also, Ψ must satisfy the restrictions that

$$
\frac{\partial \Psi}{\partial \boldsymbol{\beta}_i} = \mathbf{0} \quad \text{for} \quad \boldsymbol{\beta}_i = \mathbf{0} \tag{27}
$$

which ensure that a nonlinear form of the patch test is satisfied by the CPE.

In the remaining sections of the paper attention is limited to an isotropic compressible Neo-Hookean material which is characterized by the strain energy function

$$
\begin{aligned}
&\rho_0^*\Sigma^* = \frac{1}{2}K\big(\widetilde{J} - 1\big)^2 + \frac{1}{2}\mu\big(\overline{\alpha}_1 - 1\big)^2, \\
&\widetilde{J} = \overline{J} + \eta J, \quad \overline{J} = det(\overline{\mathbf{F}}), \quad J = det(\mathbf{F}), \quad \overline{\alpha}_1 = \overline{J}^{\,-2/3}\,\overline{\mathbf{C}} \cdot \mathbf{I}
\end{aligned}
\tag{28}
$$

where K and μ are the small deformation bulk and shear moduli, respectively, and use has been made of the work of Flory [19] to define $\overline{\alpha}_1$ as a scalar pure measure of distortional deformation. $\widetilde{J}$ is a new measure of volume change the approximates the ratio between the current volume of the element and its reference volume, and the scalar η is defined in [20]. In particular, for examples of compressible material response the quantities $\{K,\ \mu\}$ and the small deformation Poisson's ratio ν are specified by

$$K = 1\,GPa, \quad \mu = 0.6\,GPa, \quad \nu = 0.25 \tag{29}$$

whereas for nearly incompressible response these parameters are specified by

$$K = 1000\,GPa, \quad \mu = 0.6\,GPa, \quad \nu = 0.4997 \tag{30}$$

3.2 Determination of the constitutive coefficients

In [20] the strain energy of inhomogeneous deformation Ψ was taken to be a quadratic function of $\boldsymbol{\beta}_i$ which can be written in the form

$$2m\Psi = \frac{V^*\mu}{160}\sum_{i=1}^{18}\sum_{j=1}^{18} B_{ij}b_ib_j, \quad B_{ji} = B_{ij} \tag{31}$$

where the inhomogeneous strains are defined by

$$b_{(i+3(j-1))} = \boldsymbol{\beta}_j \cdot \mathbf{D}^i, \quad (i = 1, 2, 3),\ (j = 1, 2, ..., 6) \tag{32}$$

The coefficients B_{ij} can be determined by comparison with exact solutions of pure bending and adopting the nonsingular coefficients of Bubnov-Galerkin when the material becomes nearly incompressible.

4 Numerical examples

The tetrahedral CPE was implemented into the commercial finite element package ABAQUS [7] through the user subroutine UEL for the numerical study. Also, comparison is made with two ten node tetrahedral elements in ABAQUS. Predictions based on the full integration element (C3D10) are denoted by (F) and those based on the modified element (C3D10M) are denoted by (M).

For all examples, the region of the structure is meshed by rectangular bricks. A representative mesh is denoted by $\{n1,\ n2,\ n3\}$ with n_1 bricks in the $\mathbf{e}_1$ direction, n_2 bricks in the $\mathbf{e}_2$ direction and n_3 bricks in the $\mathbf{e}_3$ direction. Each brick is further meshed by dividing the brick along its diagonal to obtain two wedges, each of which is meshed with three tetrahedral elements.

4.1 Shear load on a thin cantilever beam (small deformations)

Figure 2 shows a sketch of a thin cantilever beam with rectangular cross-section defined by

$$L_1 = 200\,\text{mm}, \quad L_2 = L_3 = 10\,\text{mm} \tag{33}$$

The beam is fully clamped at its end $X_1 = 0$ and is subjected to a uniform shear stress τ applied in the $\mathbf{e}_2$ direction on its end $X_1 = L_1$. The lateral surfaces are traction free. Also, the beam is meshed by $\{20n,\, n,\, n\}$ bricks with $20n$ bricks in the $\mathbf{e}_1$ direction.

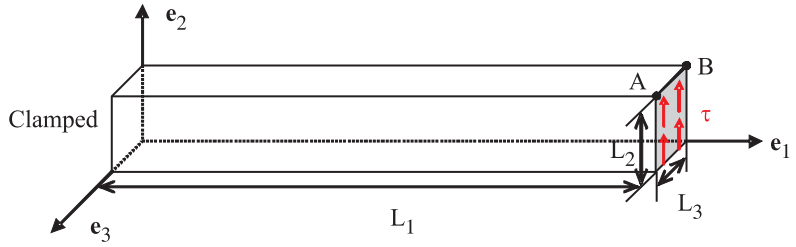

Figure 2: Uniform shear stress τ applied to the end of a thin cantilever beam.

The error E in the vertical displacement u_{A2} of the point A (Fig. 2) plotted for this example is defined by

$$E = \frac{u_{A2} - u^*_{A2}}{|u^*_{A2}|} \tag{34}$$

with the reference value u^*_{A2} being equal to the value u_{A2} predicted by the CPE with the refined mesh $(n = 10)$. Figure 3 shows the convergence of the error E of the displacement u_{A2} for the (CPE), (F) and (M) for both compressible $(\nu = 0.25)$ and nearly incompressible $(\nu = 0.4997)$ materials. Figures 3a, b check standard convergence with mesh refinement in all three directions $\{20n,\, n,\, n)$. These figures indicate that the (CPE) converges faster than (F) and (M), especially for the compressible material (Fig. 6a). Figures 6c, d examine accuracy of the elements as the elements develop very poor aspect ratios with mesh refinement only in the axial direction $\{n,\, 1,\, 1\}$. These results indicate that the (CPE) and (F) are more accurate than (M) for both compressible and nearly incompressible materials. Since Fig. 6a shows that the (CPE) is nearly converged for the mesh $\{20,\, 1,\, 1\}$, which corresponds to $n = 20$ in Fig. 6c for the compressible material, it can be concluded that the (CPE) for the compressible case is slightly more accurate than (F) and is much more accurate that (M). The results for the nearly incompressible material shown in Fig. 6d indicate that the predictions of the (CPE) are slightly less accurate than those of (F) are more accurate than those of (M).

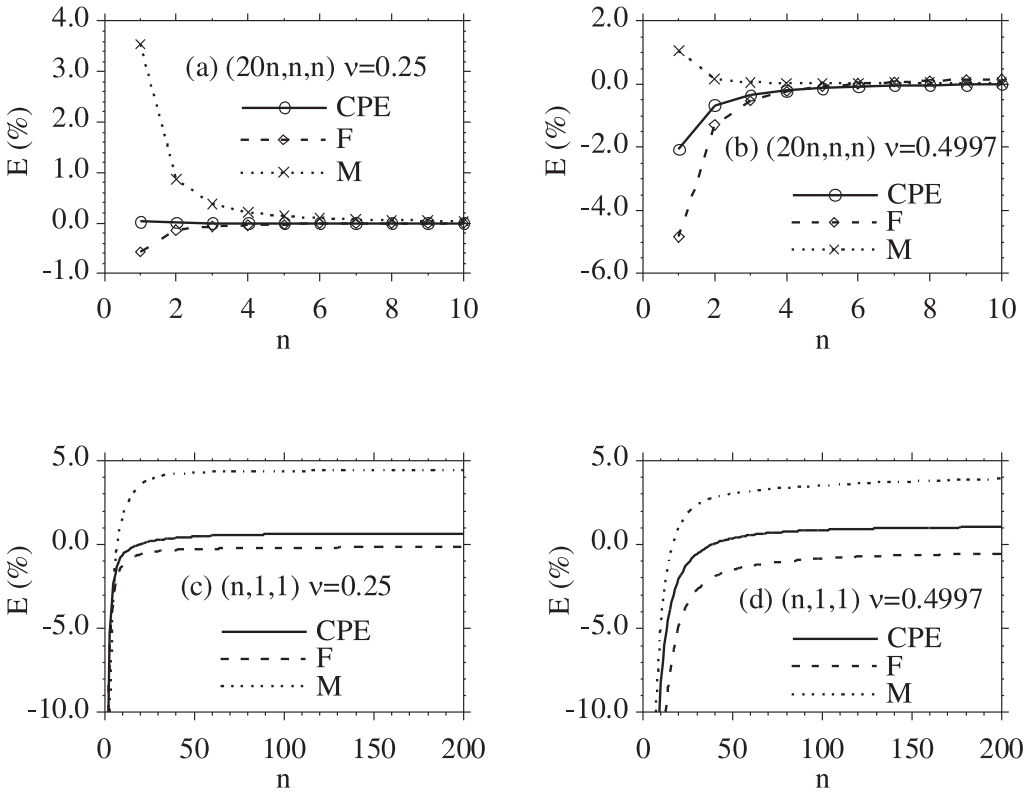

Figure 3: Shear load on a thin cantilever beam (small deformations). Convergence of the error E in the displacement u_{A2} for the (CPE), (F) and (M) elements for both compressible $(\nu = 0.25)$ and nearly incompressible $(\nu = 0.4997)$ materials with $\tau = 1\,\text{kPa}$.

4.2 Plane strain of a nearly incompressible block (large deformations)

Figure 4 shows a block with dimensions $(2L_1,\, L_2,\, L_3)$

$$L_1 = L_2 = 1.0\,\text{m}, \quad L_3 = 0.2\,\text{m} \tag{35}$$

which is loaded by a rigid plate that is perfectly bonded to half of the block's top surface $(X_2 = L_2)$. The plate remains horizontal and loads the block by moving only in the vertical direction. The edge $(X_1 = 0)$ is free to slide on a vertical plane, the bottom $(X_2 = 0)$ is free to slide on a horizontal plane, the edge $(X_1 = 2L_1)$ and the remaining top surface are traction free. This block is meshed by $\{10n,\, 5n,\, 1\}$ bricks with 10n elements in the $\mathbf{e}_1$ direction and with the depth W of the brick in the $\mathbf{e}_3$ direction given by

$$W = \frac{L_3}{n} \tag{36}$$

so that the bricks remain cubes during mesh refinement. The block is modeled as a nearly incompressible material ($\nu = 0.4997$). Although this problem is one of plane strain, since the six tetrahedral CPEs in each brick element are not arranged symmetrically the numerical solution does not predict plane strain deformations exactly.

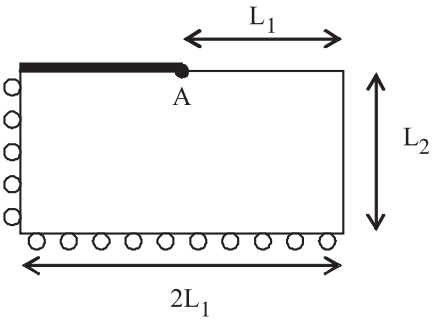

Figure 4: Plane strain of a block loaded by a rigid plate (large deformations).

For this problem let F_2 be the $\mathbf{e}_2$ component of the force applied by the plate on the block of depth L_3 and u_{A2} be the $\mathbf{e}_2$ component of the displacement of point A at the edge of the plate. The force F_2 is obtained by multiplying the vertical force applied to the plate for a block of depth W by the factor n for the refined meshes.

Figure 5 shows the force F_2 versus displacement u_{A2} of the plate for the $\{(CPE),$ $(F),$ $(M)\}$ for the coarse mesh $\{10,\ 5,\ 1\}$ (i.e. $n = 1$) and for the (CPE) with refined mesh $\{100,\ 50,\ 1\}$ (i.e. $n = 10$) denoted by (CPE^*). The values of the last points of convergence depend slightly on the final displacements specified for the calculations, which were taken to be $u_{A2}/L_1 = 1.50$ and -0.75, respectively for tension and compression. These last points of convergence are denoted by symbols in Fig. 5. Moreover, from Fig. 5 it can be seen that all of the solutions for the coarse mesh $\{10,\ 5,\ 1\}$ are relatively accurate in the range of convergence of the refined mesh $\{100,\ 50,\ 1\}$. It can also be seen that the (CPE) exhibits more robust response than (F) and (M) in tension and less robust response than these elements in compression, and that the response predicted by (F) in compression is too stiff.

Specifically, Figs. 6 and 7 show the deformed shapes of the (CPE) and (M) for the last points of convergence in tension and compression, respectively. From these figures it can be seen that the (CPE) predicts stable response, whereas (M) exhibits instabilities in both tension and compression. The instability is clearly seen in Fig. 6b and 7b near the free edges.

4.3 Indentation of a smooth rigid sphere into a block (large deformations)

Figure 8 shows a sketch of indentation of a smooth rigid sphere into a nearly incompressible ($\nu = 0.4997$) block. The total length $2L_1$, total depth $2L_2$, total height L_3 of

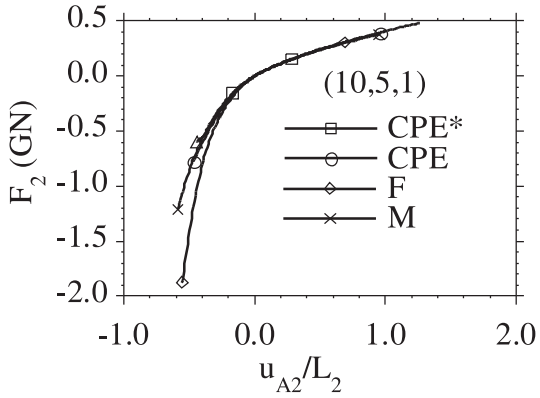

Figure 5: Plane strain extension and compression of a nearly incompressible block loaded by a rigid plate (large deformations). Force F_2 versus displacement u_{A2} of the plate for the $\{(CPE),\ (F),\ (M)\}$ with the coarse mesh $\{10,\ 5,\ 1\}$ and (CPE^*) with the refined mesh $\{100,\ 50,\ 1\}$. The last points of convergence are marked by symbols.

the block and the radius R of the spherical punch are specified by

$$L_1 = L_2 = L_3 = 1.0\,\mathrm{m}, \quad R = 0.5\,\mathrm{m} \tag{37}$$

The bottom $(X_3 = 0)$ of the block remains in contact and slides freely on the plane $(X_3 = 0)$ and the remaining surfaces of the block are traction free except at the points of contact of the rigid spherical punch with the deformed top surface $(X_3 = L_3)$. The rigid punch can only move vertically with displacement u_3 in the $\mathbf{e}_3$ direction. Moreover, only one fourth of the block is analyzed and is modeled by the mesh $\{5n,\ 5n,\ 5n\}$ of bricks. Also, use is made of symmetry planes for $X_1 = 0$ and $X_2 = 0$.

The vertical force F_3 applied to one quarter of the punch and the vertical displacement u_{A3} of the point A of the punch are plotted in Fig. 9 for the (CPE) and (M) with two different meshes. In this regard, it is noted that ABAQUS does not allow the use of (F) for contact problems. Figure 9 shows that the refined meshes $(n = 5)$ of both the (CPE) and (M) predict nearly identical results and the coarse mesh $(n = 1)$ of the (CPE) is very accurate. The (CPE) with the refined mesh $(n = 5)$ converged for the full range of deformation shown in Fig. 9 and ceased to converge at $u_{A3}/L_3 = -0.46403$ for the coarse mesh $(n = 1)$. In contrast, the element (M) ceased to converge for the coarse mesh (n=1) at $u_{A3}/L_3 = -0.41264$ and for the refined mesh $(n = 5)$ at $u_{A3}/L_3 = -0.41337$. These points where the elements ceased to converge in marked by symbols in Fig. 9. These results indicate that the (CPE) is more robust that (M).

Moreover, Fig. 10 shows the deformed shape predicted by the (CPE) with the refined mesh $(n = 5)$ for $u_{A3}/L_3 = -0.5$, both with and without the spherical punch.

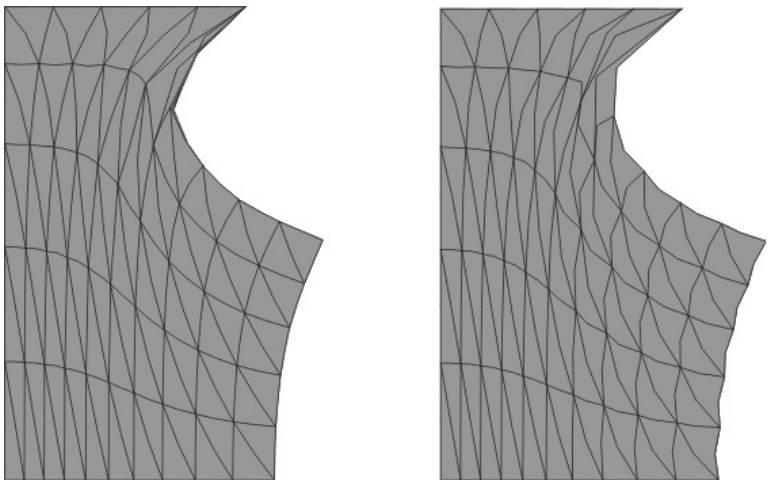

(a) CPE (u_{A2}/L_2= 0.9633) (b) M (u_{A2}/L_2= 0.9520)

Figure 6: Plane strain extension of a nearly incompressible block loaded by a rigid plate (large deformations). Deformed shapes predicted by the (CPE) and the modified element (M) for tension with the coarse mesh $\{10,\ 5,\ 1\}$ at the last point of convergence associated with the displacement u_{A2}/L_2.

5 Conclusion

In the previous sections a ten node tetrahedral Cosserat Point Element (CPE) has been discussed for large deformations of nonlinear isotropic hyperelastic materials. The constitutive equations treat the CPE as a structure and the kinetic quantities are determined by hyperelastic equations as derivatives of the strain energy function. In particular, these constitutive equations are algebraic and no integration is required over the element region.

Examples of a thin cantilever beam, plane stain deformations of a block and indentation of a smooth rigid spherical punch into a three-dimensional block show that the resulting tetrahedral CPE is accurate, robust and is valid for thin structures as well as three-dimensional bodies. Also, the CPE can be used for contact problems and it exhibits a smooth transition from compressible to nearly incompressible material behaviour.

References

[1] O. Klaas, A. Maniatty, M.S. Shephard, "A stabilized mixed finite element method for finite elasticity. Formulation for linear displacement and pressure interpolation", Comp. Meth. in Appl. Mech. and Engng, 180, 65-79, 1999.

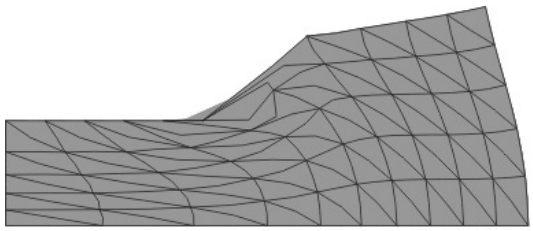

(a) CPE ($u_{A2}/L_2 = -0.4666$)

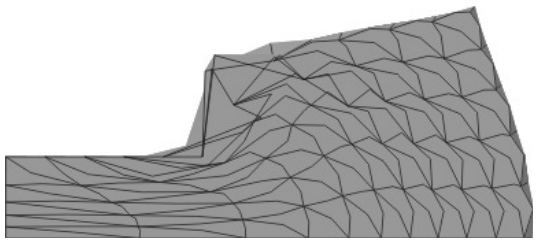

(b) M ($u_{A2}/L_2 = -0.5862$)

Figure 7: Plane strain compression of a nearly incompressible block loaded by a rigid plate (large deformations). Deformed shapes predicted by the (CPE) and the modified element (M) for compression with the coarse mesh $\{10,\ 5,\ 1\}$ at the last point of convergence associated with the displacement u_{A2}/L_2.

[2] R.L. Taylor, "A mixed-enhanced formulation for tetrahedral finite elements", Int. J. for Numer. Meth. in Engng, 47, 205-227, 2000.

[3] R. Cisloiu, M. Lovell, J. Wang, "A stabilized mixed formulation for finite strain deformation for low-order tetrahedral solid elements", Finite Elements in Analysis and Design, 44, 472-482, 2008.

[4] M. Chiumenti, Q. Valverde, C. Agelet de Saracibar, M. Cervera, "A stabilized formulation for incompressible elasticity using linear displacement and pressure interpolations", Comp. Meth. in Appl. Mech. and Engng, 191, 5253-5264, 2002.

[5] M. Cervera, M. Chiumenti, Q. Valverde, C. Agelet de Saracibar, "Mixed linear/linear simplicial elements for incompressible elasticity and plasticity", Comp. Meth. in Appl. Mech. and Engng, 192, 5249-5263, 2003.

[6] E. Onate, J. Rojek, R.L. Taylor, O.C. Zienkiewicz "Finite calculus formulation for incompressible solids using linear triangles and tetrahedra" Int. J. for Numer. Meth. in Engng, 59, 1473-1500, 2004.

[7] ABAQUS, Version 6.10.3, ABAQUS, Providence, RI.

[8] S.H. Lo, C. Ling, "Improvement on the 10-node tetrahedral element for three-dimensional problems", Comp. Meth. in Appl. Mech. and Engng, 189, 961-974, 2000.

[9] M.B. Rubin, "On the theory of a Cosserat point and its application to the numerical solution of continuum problems", ASME J. of Appl. Mech., 52, 368-372,

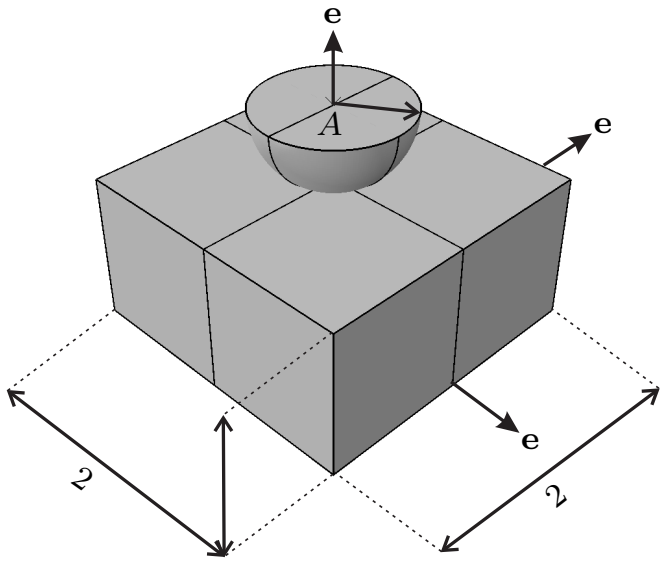

Figure 8: Indentation of a smooth rigid sphere into a nearly incompressible block (large deformations).

1985.

[10] M.B. Rubin, "On the numerical solution of one-dimensional continuum problems using the theory of a Cosserat point", ASME J. of Appl. Mech., 52, 373-378, 1985.

[11] M.B. Rubin, "Numerical solution of two- and three-dimensional thermomechanical problems using the theory of a Cosserat point", J. Math. Phys ZAMP, 46, Special Issue S308-S334. In: Casey J., Crochet, M.J. (Eds.), Theoretical, Experimental, and Numerical Contributions to the Mechanics of Fluids and Solids, Birkhauser Verlag, Basel, 1995.

[12] M.B. Rubin "Cosserat Theories: Shells, Rods and Points, Solid Mechanics and its Applications", Kluwer, The Netherlands. Vol. 79, 2000.

[13] B. Nadler, M.B. Rubin, "A new 3-D finite element for nonlinear elasticity using the theory of a Cosserat point", Int. J. Solids Struct., 40, 4585-4614, 2003.

[14] S. Loehnert, E.F.I. Boerner, M.B. Rubin, P. Wriggers, "Response of a nonlinear elastic general Cosserat brick element in simulations typically exhibiting locking and hourglassing", Comp. Mech., 36, 255-265, 2005.

[15] M. Jabareen, M.B. Rubin, "Hyperelasticity and physical shear buckling of a block predicted by the Cosserat point element compared with inelasticity and hourglassing predicted by other element formulations", Computational Mechanics 40, 447-459, 2007.

[16] M. Jabareen, M.B. Rubin, "An improved 3-D Cosserat brick element for irregular shaped elements", Comp. Mech., 40, 979-1004, 2007.

[17] M. Jabareen, M.B. Rubin, "A generalized Cosserat point element (CPE) for isotropic nonlinear elastic materials including irregular 3-D brick and thin structures", J. of Mech. of Materials and Struct., 3, 1465-1498, 2008.

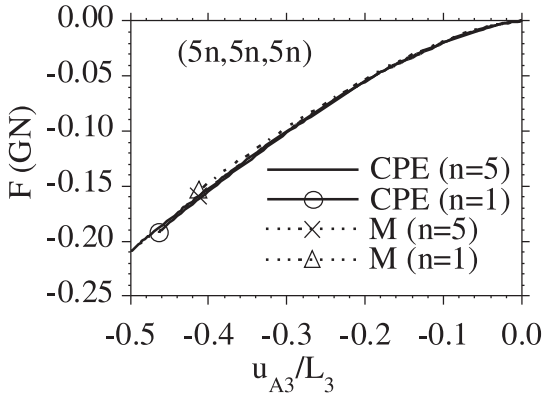

Figure 9: Indentation of a smooth rigid sphere into a nearly incompressible block (large deformations). Force F versus displacement u_{A3} predicted by the (CPE) and (M) for the mesh $\{5n,\ 5n,\ 5n\}$. The symbols denote the last points of convergence of the (CPE) for $n = 1$ and (M) for $n = 1$ and 5.

[18] A.E. Gree, J.E. Adkins "Large elastic deformations and non-linear continuum mechanics", Oxford, 1961.

[19] P. Flory, "Thermodynamic Relations For High Elastic Materials", Trans. Faraday Soc., 57, 829-838, 1961.

[20] E. Hanukah, "Development of a higher order tetrahedral Cosserat point element (CPE) for nonlinear elasticity", Master Thesis, Technion - Israel Institute of Technology, 2012.

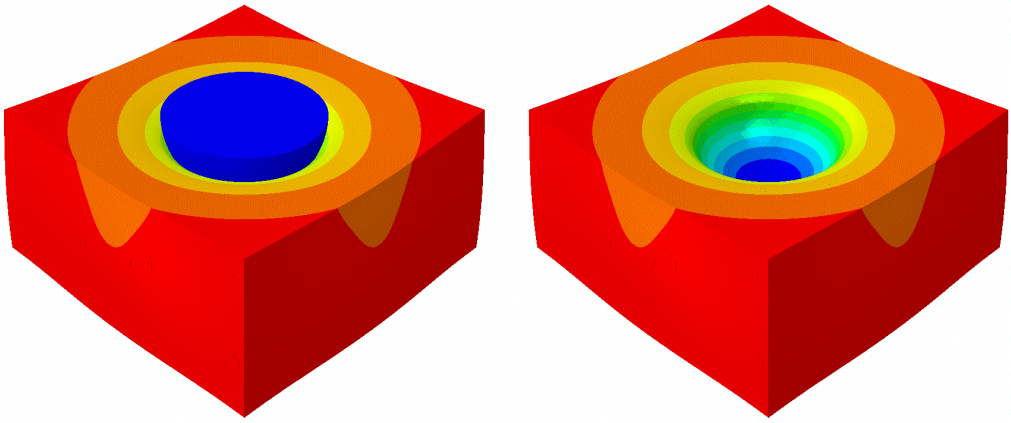

Figure 10: Indentation of a smooth rigid sphere into a nearly incompressible block (large deformations). Deformed shape predicted by the (CPE) with the refined mesh $\{25,\ 25,\ 25\}$ for $u_{A3}/L_3 = -0.5$, both with and without the spherical punch.